*fire*

MDPI

*Article*

# Comparative Study on Residual Capacity of Fire-Damaged Rectangular and T-Shaped Concrete Beams

**Manish K. Sah [1], Pratik Bhatt [2], Vasant A. Matsagar [3], Heesun Kim [4] and Venkatesh K. R. Kodur [1,4,*]**

[1] Department of Civil and Environmental Engineering, Michigan State University, East Lansing, MI 48824, USA; sahmanis@msu.edu
[2] Engineering Systems Inc. (ESi), Aurora, IL 60504, USA; ppbhatt@engsys.com
[3] Department of Civil and Environmental Engineering, Indian Institute of Technology (IIT) Delhi, New Delhi 110 016, India; matsagar@civil.iitd.ac.in
[4] Architectural and Urban Systems Engineering, Ewha Womans University, Seoul 03760, Republic of Korea; hskim3@ewha.ac.kr
* Correspondence: kodur@egr.msu.edu

**Abstract**

In this study, the comparative residual performance of fire-exposed reinforced concrete (RC) beams with rectangular and T-shaped cross-sections is investigated. Two concrete beams, one with a T-section and the other with a rectangular section, were tested under the combined effects of fire exposure and structural loading. Data generated in the tests during and following fire exposure is utilized to compare the thermal and structural response of the beams. The results indicate a notable difference in the temperature evolution, mid-span deflection, and the residual capacity of the beams. The T-beam experienced greater deflection and stiffness degradation due to its larger exposed surface area (approximately 17% higher than the rectangular beam) and flange geometry, despite comparable peak rebar temperatures. A simplified approach, based on the maximum concrete and rebar temperatures and corresponding strength reductions, is proposed to evaluate the residual capacity of fire-exposed RC beams. For equal cover depth to reinforcement, peak rebar temperature is unaffected by cross-section shape as long as the web of the T-beam is not slender. T-shaped beams with similar overall depth exhibit greater post-fire strength retention than rectangular beams when the neutral axis lies within the flange. A 20% reduction in the web thickness and a combined reduction of 20% in web and 37% in flange thickness result in a comparable decrease in the flexural capacity to that of the rectangular beams of similar depth, indicating that the flange plays a key role in maintaining post-fire performance.

**Keywords:** reinforced concrete; standard fire; fire damaged beam; residual capacity; structural response

Check for updates

Academic Editors: Lu He, Guowei Zhang and Tianwei Chu

Received: 8 February 2026
Revised: 2 March 2026
Accepted: 9 March 2026
Published: 12 March 2026

**Copyright:** © 2026 by the authors. Licensee MDPI, Basel, Switzerland. This article is an open access article distributed under the terms and conditions of the Creative Commons Attribution (CC BY) license.

## 1. Introduction

Fire is a common and potentially destructive hazard that affects the safety and performance of structural members. When exposed to fire, structural members experience a loss in strength and stiffness due to the rise in cross-sectional temperature of the constituent materials. To mitigate this adverse effect, structural members are required to be provided with appropriate fire resistance provisions as specified by building codes [1], ensuring life safety, stability, and structural integrity. Consequently, fire-induced structural collapse in reinforced concrete (RC) structures is very rare due to concrete's low thermal conductivity,

high specific heat, and slower degradation of its mechanical properties [2]. However, concrete structures might experience a certain level of fire damage, which can reduce the capacity of the members following a fire. Assessing the residual capacity of RC members following fire exposure is essential for evaluating structural damage, ensuring safety, and determining appropriate repair strategies. Past events have demonstrated that, with proper inspection and rehabilitation, most fire-damaged RC structures can be safely restored and reoccupied [3,4].

According to Kodur and Agrawal (2016) [5], the residual capacity of fire-damaged reinforced concrete (RC) structures is influenced by several factors, including structural geometry, fire exposure duration and severity, temperature-dependent material properties, applied load, and boundary conditions. Among common RC configurations, T-shaped beams are increasingly used due to their structural efficiency and ability to reduce overall floor depth. However, their geometry with relatively thin flanges and webs makes them more susceptible to strength degradation and the onset of instability under fire conditions. This can significantly affect their residual capacity of T-beams after fire exposure [6].

Previous studies have shown that the residual capacity of fire-exposed RC structures can be evaluated using testing under laboratory conditions, simplified analytical methods, or finite element analysis [7,8]. Agrawal and Kodur (2020) [9] proposed a novel three-stage (pre-fire exposure condition, during fire exposure comprising heating and cooling phases of fire, and post-fire exposure conditions) experimental approach and applied it to RC rectangular beams exposed to ASTM E119 fire curve with heating durations of 90 min and 120 min and load conditions. The findings revealed that rectangular beams retained considerable residual strength; however, they exhibited large post-fire deformations, affecting serviceability. Liu et al. (2021) [10] tested ten RC T-beams under three different load levels (i.e., 0, 12%, and 44%), and the ISO 834 standard fire curve with heating durations of 60 min, 90 min, and 120 min, followed by residual flexural capacity evaluation using experiments and FE modeling in ANSYS. The results showed that higher load ratios and longer fire exposure led to greater crack development, increased deflections, and up to 20% strength loss, with stiffness degradation being more significant than strength loss. Liu et al. (2023) [11] developed a calculation method combining the FE thermal modeling and equilibrium analysis to estimate the residual capacity of fire-damaged T-beams, incorporating fire-induced cracking. Their findings show that crack effects significantly influence post-fire capacity on concrete beams. In addition to analytical developments on beam behavior, experimental investigations on other structural members have further emphasized the importance of cooling conditions in post-fire assessment. Awad et al. (2022) [12] investigated the influence of different cooling schemes on the ultimate strength of RC columns and demonstrated that both fire severity and cooling methods significantly affect strength degradation and stiffness loss. Their findings highlight the critical role of the cooling phase and internal temperature evolution in determining post-fire capacity.

Recent work by Wang et al. (2024) [13] investigated the fire performance of several prestressed concrete T-beams subjected to varying fire durations, using both finite element and simplified analytical methods. Their results showed up to 93 percent loss in prestress and a 28 percent reduction in load-carrying capacity. Although several studies have evaluated the fire performance and residual capacity of rectangular beams and T-shaped beams independently, direct and normalized comparisons between these two cross-sectional configurations under identical fire exposure and loading conditions remain limited. Moreover, existing simplified post-fire assessment approaches are typically validated for a single geometry and do not explicitly isolate geometry-driven effects. Therefore, a systematic comparative framework is required to clearly distinguish the influence of section configuration on post-fire residual behavior.

The objective of this study is to compare the post-fire residual performance of reinforced concrete beams with T-shaped and rectangular cross-sections. To achieve this, two beams of similar depth, one T-shaped and the other rectangular, were tested under standard fire exposure to examine their thermal and structural responses during and after fire. In addition, a simplified approach is proposed to predict the residual strength of fire-exposed RC beams, providing a practical tool for post-fire evaluation and repair strategies.

## 2. Response of RC Beam During Fire Exposure

Figure 1 illustrates the typical structural response of a reinforced concrete (RC) beam prior to fire exposure, during fire exposure, and after cooling down following fire exposure. The RC beam undergoes three distinct phases during and after a fire: the heating phase, the cooling phase, and the residual phase. After flashover, cross-sectional temperatures gradually rise, leading to a reduction in load-carrying capacity and an increase in deflection due to degradation in the strength and stiffness properties of both concrete and reinforcement. Even as the fire temperature begins to decrease during the cooling phase, internal temperatures within the member remain elevated for an extended period due to the high thermal inertia of concrete. Depending on the member's size (thermal mass) and the severity of the fire, it may take 24 to 72 h for temperatures in the concrete core to return to ambient levels after fire extinguishment. Once the member cools to ambient conditions, residual deflection is typically observed. This unrecoverable deformation (as seen in Figure 1) reflects the extent of structural damage sustained during the fire and serves as a key indicator of the beam's residual capacity [14].

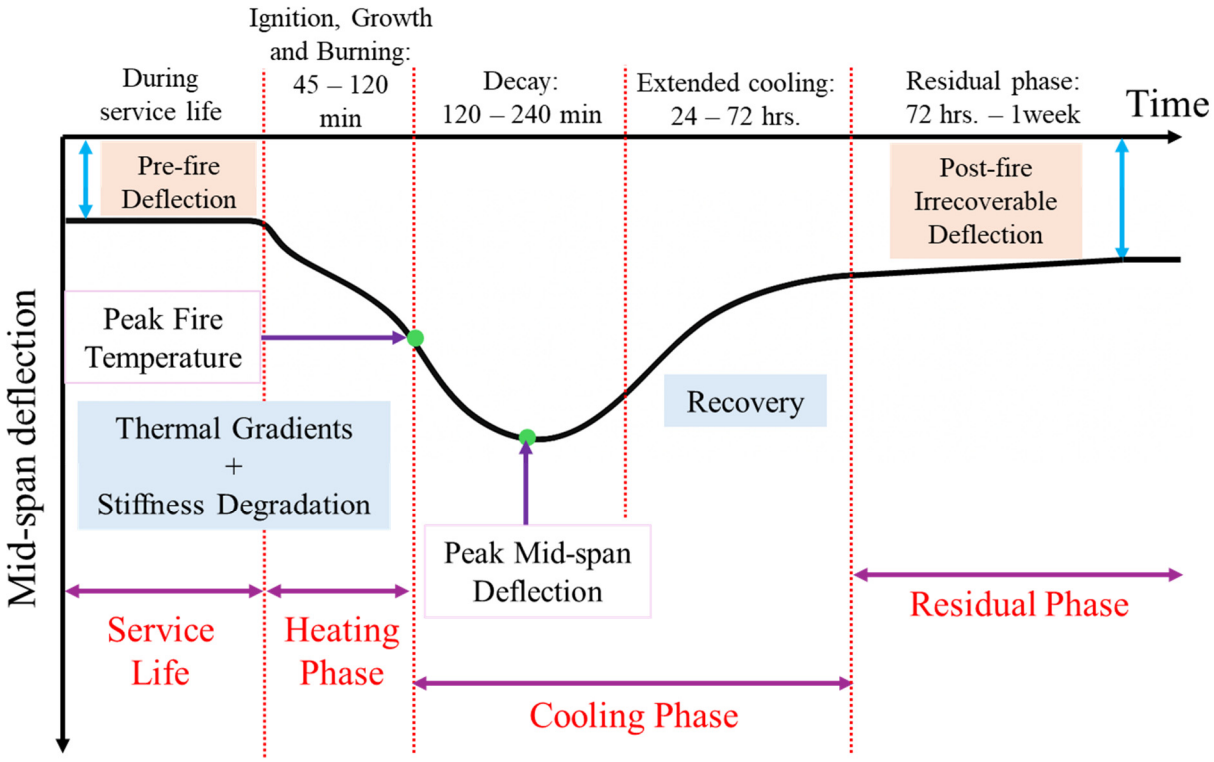



**Figure 1.** Structural response of a typical RC beam prior to and post-fire exposure.

The residual capacity of a fire-exposed reinforced concrete (RC) beam is influenced by several factors, including the internal temperature distribution during fire exposure, the applied load level, peak temperature attained, boundary conditions, cooling rate, cooling method, and the duration of post-fire strength recovery. Although the cooling method (air cooling or water quenching) has a limited impact on the post-fire compressive strength of

concrete, it significantly affects the failure strain and elastic modulus [15]. Concrete that is quenched typically exhibits a higher compressive strain at failure compared to concrete cooled gradually under ambient conditions. Apart from these factors, the cross-sectional geometry of the members also significantly affects the residual capacity and performance of the beam. However, as indicated in the previous section, there are no studies quantifying the effect of cross-section geometry on the post-fire residual capacity of concrete beams. Therefore, post-fire residual capacity tests are performed on beams of rectangular and T-shaped cross-section; the details of the tests are described in the following sections.

## 3. Experimental Program

As part of the experimental program, two beams, one rectangular beam designated as B1 and a T-shaped beam designated as TB1, were tested under the combined effect of structural and fire loading. Data from the tests is utilized to compare the thermal and structural response of these beams under three stages, namely, prior to fire exposure, during fire exposure, and post-fire exposure conditions, respectively.

### *3.1. Fabrication of Test Beams*

Two concrete beams were fabricated at the Civil Infrastructure Laboratory (CIL) of Michigan State University (MSU). Figure 2 illustrates the fabrication process, where Figure 2a shows the steel cage and Figure 2b shows the finished concrete surface after casting. The detailed batch mix proportions for both beams are summarized in Table 1, along with the measured compressive strengths at 28 days and on the day of testing. The average compressive cylinder strengths, determined from three specimens per batch, were 58 MPa and 62 MPa for the B1 beam, and 38 MPa and 48 MPa for the TB1 beam at 28 days and test day, respectively. The higher compressive strength of the B1 beam is attributed to the addition of a water-reducing admixture, which lowered the overall water/cement ratio; in addition, the air content of the B1 concrete was also lower than that of the TB1 concrete. The continued gain in compressive strength beyond 28 days can be attributed to the sustained hydration of the cementitious matrix. The 28-day splitting tensile strengths of the B1 and TB1 concretes were 3.7 MPa and 2.8 MPa, respectively.

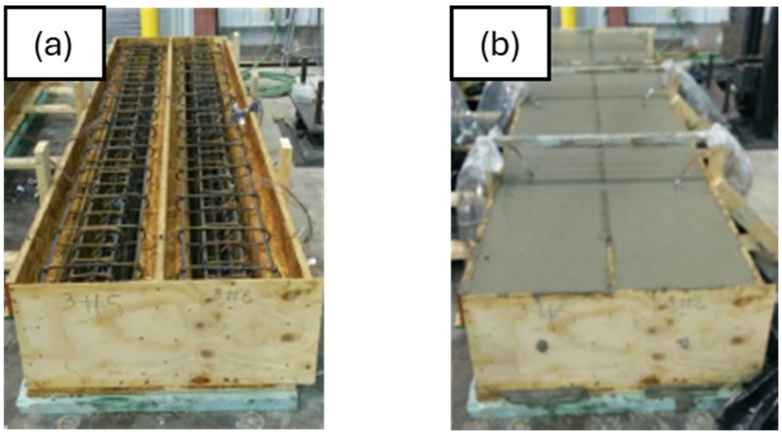



**Figure 2.** Fabrication of beams: (**a**) steel cage, (**b**) finished surface after concrete pour.

**Table 1.** Batch mix proportions used in the fabrication of RC beams.

| Mix Design | Beam | |
|---|---|---|
| | **B1** | **TB1** |
| Cement (kg/m$^3$) | 389.9 | 335 |
| Water (kg/m$^3$) | 156.4 | 151 |
| Coarse aggregate (kg/m$^3$) | 1036.9 | 1032 |
| Fine aggregate (kg/m$^3$) | 830.1 | 790 |
| Portland cement type | Type I | Type I |
| Coarse aggregate type | Carbonate | Carbonate |
| Fine aggregate type | Natural sand | Natural sand |
| Water reducing agent (kg/m$^3$) | 1.9 | - |
| Slump (mm) | 100 | 100 |
| Water/cement ratio | 0.4 | 0.45 |
| Air content (%) | 1.7 | 5.5 |
| Unit weight (kg/m$^3$) | 2415 | 2410 |
| Split tensile strength—28th day (MPa) | 3.7 | 2.8 |
| Compressive strength—28th day (MPa) | 58 | 38 |
| Compressive strength—test day (MPa) | 62 | 48 |

The beam dimensions were selected based on the constraints of the fire-testing furnace and loading setup. Both the normal-strength concrete (NSC) rectangular and T-shaped beams were designed in accordance with ACI 318 provisions (ACI, 2019) [16], and their geometric details are provided in Table 2. Plywood molds were prepared for casting, followed by the placement of the reinforcement cages. Ready-mix concrete supplied from a local batching plant was used for fabrication, and the beam surfaces were leveled and finished after casting. The specimens were kept in the molds for 7 days to allow initial curing and were subsequently stored under ambient laboratory conditions of approximately 25 °C temperature and 40% relative humidity until testing.

**Table 2.** Geometric details of RC beams for fire resistance tests.

| Property | Beam | |
|---|---|---|
| | **B1** | **TB1** |
| Length (m) | 3.96 | 3.96 |
| Cross-section, width × height (mm) | 254 × 406 | Flange: 432 × 127<br>Web: 254 × 279 |
| Longitudinal rebar diameter | Top: 2–13 mm ϕ<br>Bottom: 3–19 mm ϕ | Top: 4–12 mm ϕ<br>Bottom: 3–16 mm ϕ |
| Transverse rebar diameter | - | 10 mm ϕ @ 305 mm c/c |
| Stirrup rebar diameter | 6 mm ϕ @ 150 mm c/c | 10 mm ϕ @152 mm c/c |
| Concrete cover (mm) | Top: 50; Bottom: 38<br>Left: 38; Right: 38 | 38 |

The design and actual room temperature moment capacities are calculated according to ACI 318 for the rectangular (B1) and T-shaped (TB1) beams. The design capacity was determined using the design yield strength of the steel reinforcement and the design compressive strength of concrete. The actual capacity was calculated using the measured strengths of concrete and steel reinforcement obtained from laboratory testing at Michigan State University (MSU) without using a strength reduction factor. For the B1 beam, both

the design and actual moment capacities were calculated and found to be 121 kNm and 129 kNm, respectively. For the TB1 beam, the design and actual moment capacities were calculated as 89 kNm and 95 kNm, respectively.

### *3.2. Instrumentation*

The tested beams were instrumented with Type-K chromel–alumel thermocouples and linear variable displacement transducers (LVDTs) to monitor thermal and structural responses during testing. Type-K thermocouples with a wire diameter of 0.91 mm were embedded to monitor temperature development in both the reinforcement and concrete at three cross-sections along the span of the reinforced concrete beams. Figures 3 and 4 show the elevation views and thermocouple locations for the B1 and TB1 beams. In Figures 3b and 4b, Sections A-A and C-C indicate thermocouple locations at the loading points, while Section B-B represents the mid-span. The locations of Sections A-A, B-B, and C-C for the B1 and TB1 beams are shown in Figures 3a and 4a, respectively. The notations TC1 to TC15 in Figures 3b and 4b indicate the locations of the thermocouples. Beam deflections were measured using three linear variable displacement transducers (LVDTs), placed at the mid-span and at the two loading points.

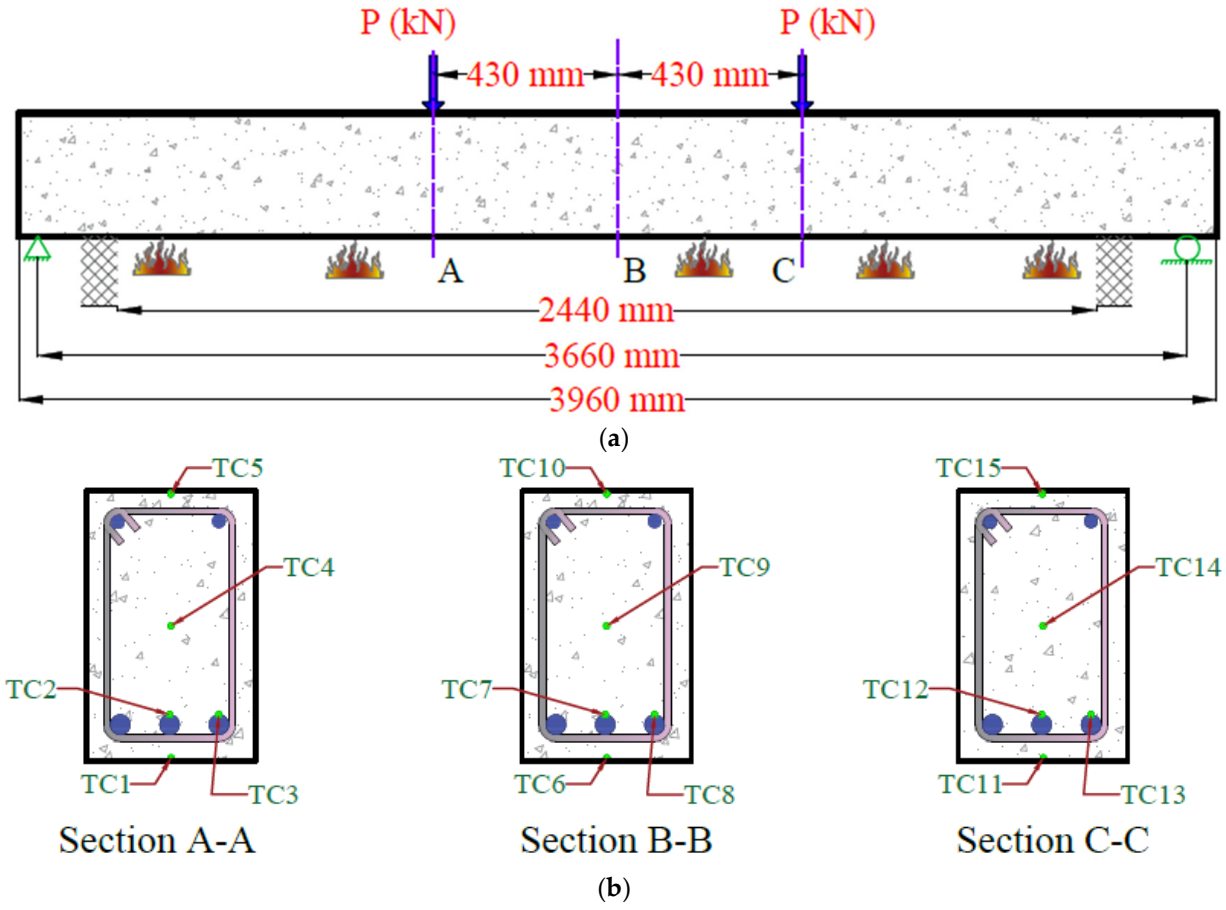



**Figure 3.** Beam setup and instrumentation of rectangular section beam B1: (**a**) elevation view, (**b**) thermocouple locations.

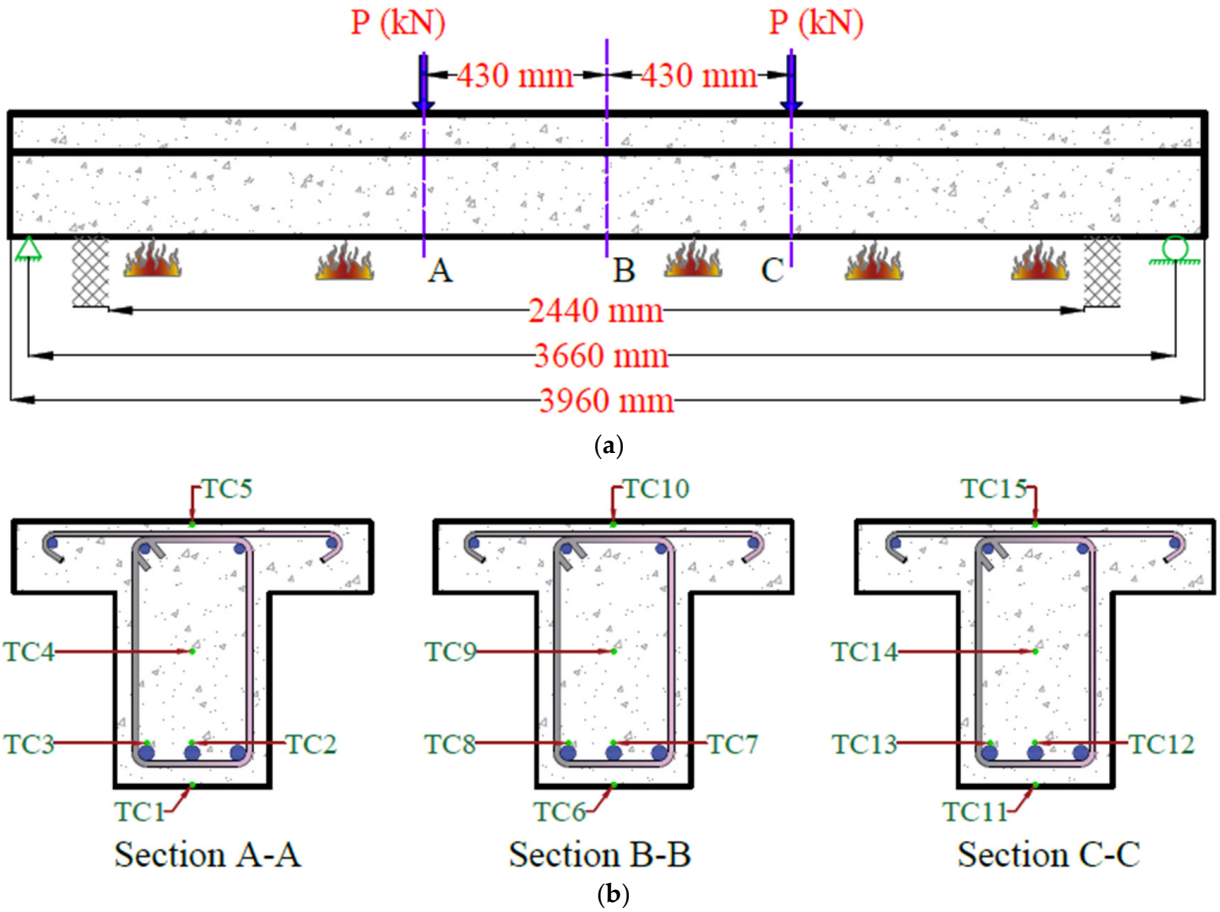



**Figure 4.** Beam setup and instrumentation of T-beam TB1: (**a**) elevation view, (**b**) thermocouple locations.

### *3.3. Fire Test Furnace*

Two different fire resistance tests were conducted using the structural fire testing furnace at the Civil Infrastructure Laboratory of Michigan State University (MSU), shown in Figure 5. To replicate realistic fire conditions, the furnace is integrated with a loading frame that allows simultaneous application of heat and structural load. The loading frame consists of steel beams and columns that provide real-time support and loading conditions. The furnace has a steel frame supported by four columns and includes a fire chamber measuring 3.05 m in length, 2.44 m in width, and 1.78 m in height. Six natural gas burners, capable of producing up to 2.5 MW of heat, are mounted on the furnace walls to ensure uniform heat distribution. Six Type-K chromel–alumel thermocouples are installed on the interior walls to monitor furnace temperatures. Gas input and ventilation are manually controlled to maintain furnace temperatures according to the desired fire curve. All sensors, including thermocouples, linear variable differential transducers (LVDTs), and load cells, are connected to a data acquisition system for real-time monitoring and recording of temperature, displacement, and load.

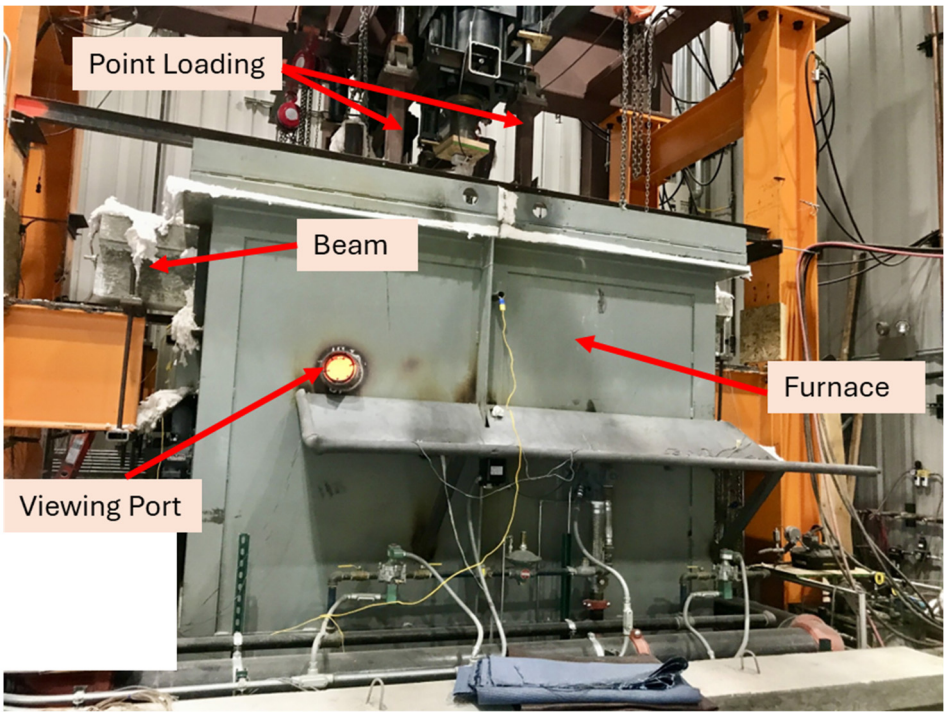



**Figure 5.** Fire test setup at MSU Civil Infrastructure Laboratory.

### *3.4. Test Conditions and Procedure*

The fire resistance tests of the RC beams were conducted under predetermined fire exposure, loading, and boundary conditions. Both beams were tested under simply supported end conditions and subjected to four-point flexural loading. The loads were applied at approximately 1.4 m from each support to produce pure flexural behavior in the region between the loading points, as shown in Figures 3a and 4a. The B1 and TB1 beams were loaded to approximately 55% and 50% of their flexural capacities, respectively, as calculated using ACI 318 provisions (ACI Committee, 2008) [17]. The load was applied and held for 30 min prior to fire exposure to stabilize deflections.

In fire testing, the duration of heating is often used to distinguish between short and long fire exposures. Short-duration curves typically represent heating up to about 90 min, while long-duration curves extend to about 120 min and beyond [9]. In this study, only the long-duration fire curves were used. The B1 and TB1 beams were exposed to the long-duration fire curves (LF1 and LF2), respectively, as shown in Figure 6. During the fire tests, the beams were exposed to fire on three surfaces, i.e., the bottom soffit and two sides up to a length of 2440 mm for a duration of 120 min following the ASTM E119 standard fire curve. The LF1 curve closely follows the standard fire curve, while LF2 shows lower temperatures during the heating phase due to the failure of one burner after the test began. However, the resulting temperature difference between the LF1 and LF2 curves was generally less than about 100 °C, and this variation is considered small and not expected to have a significant influence on the post-fire structural performance of the beams. During the cooling phase, LF2 exhibited a slower temperature drop compared to LF1 because the cooling fan was turned off to simulate natural cooling. Table 3 summarizes the test parameters for both beams. Various output parameters, including temperature distribution, mid-span deflection, and residual capacity, were recorded during the test and are used to evaluate performance in the following section.

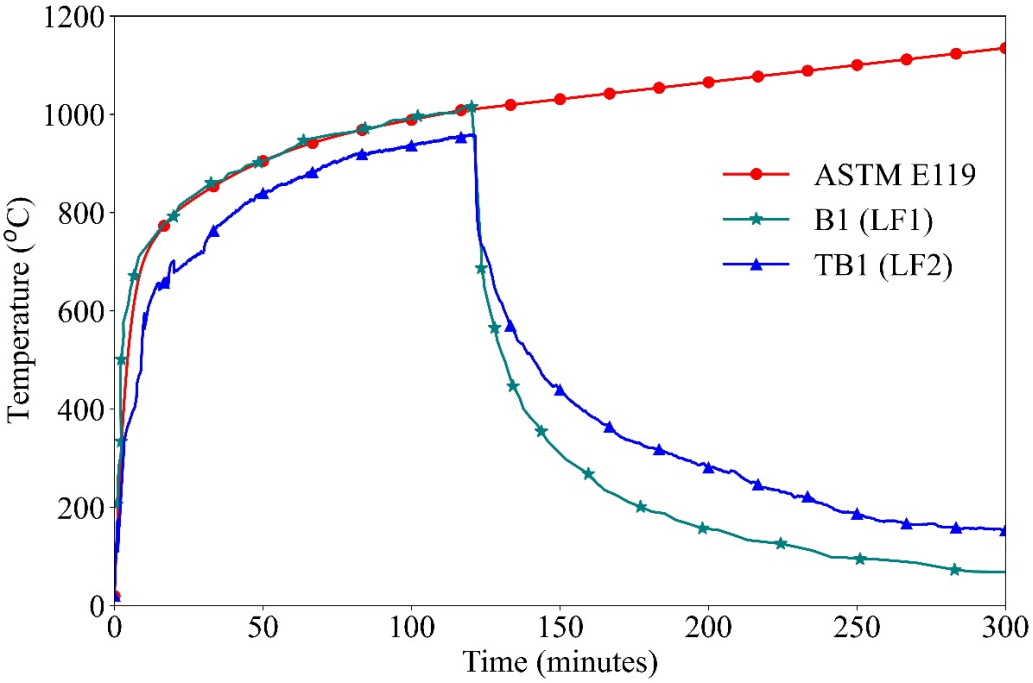



**Figure 6.** Time–temperature curves showing heating and cooling phases of the fire scenario used in the test.

**Table 3.** Test parameters and results for NSC beams.

| Parameters | Beam | |
|---|---|---|
| | **B1** | **TB1** |
| Fire exposure | LF1 (120 min heating) | LF2 (120 min heating) |
| Support conditions | SS | SS |
| Load applied before fire (minutes) | 30 | 30 |
| *P* (kN) (ratio to nominal capacity, %) | 50 (55%) | 32 (50%) |
| Relative humidity (%) | 89.8 | 92 |
| Measured fire resistance | NF | NF |
| Predicted fire resistance (minutes) | 90 | 90 |
| Spalled volume ratio (%) | 0.1 | 0.6 |
| Extent of spalling | Minor | Minor |

NF: no failure; SS: simply supported; LF: long-duration fire.

## 4. Comparative Fire Performance of Beams

The generated test data are used to evaluate the comparative fire response of rectangular and T-shaped beams, with emphasis on the influence of beam geometry on post-fire residual capacity. The extent of spalling in the B1 and TB1 beams was 0.1% and 0.6%, respectively, both remaining below 2%, which indicates minor spalling. The slightly higher spalling in the TB1 beam is attributed to its larger exposed surface area resulting from the flange. The overall response of the beams is evaluated in three stages: prior to fire exposure, during fire exposure, and after fire exposure.

### *4.1. Just Prior to Fire Exposure*

The measured pre-fire mid-span deflection (during service life) for both beams is presented in Table 4. In both cases, deflection increased steadily with the applied load, exhibiting an almost linear trend until the onset of tensile cracking. This cracking was primarily localized within the critical region between the two point loads, where a constant bending moment induced high flexural stresses. The higher mid-span deflection observed

in the B1 beam is attributed to the greater applied load. After reaching peak load, the applied load was maintained for 30 min to allow deflections to stabilize before initiating fire exposure.

**Table 4.** Pre-fire response of RC beams.

| Parameters | Beam | |
|---|---|---|
| | **B1** | **TB1** |
| Nominal capacity, *P* (kN) | 50 (55%) | 32 (50%) |
| Support conditions | SS | SS |
| Mid-span deflection (mm) | 5.5 | 3.2 |

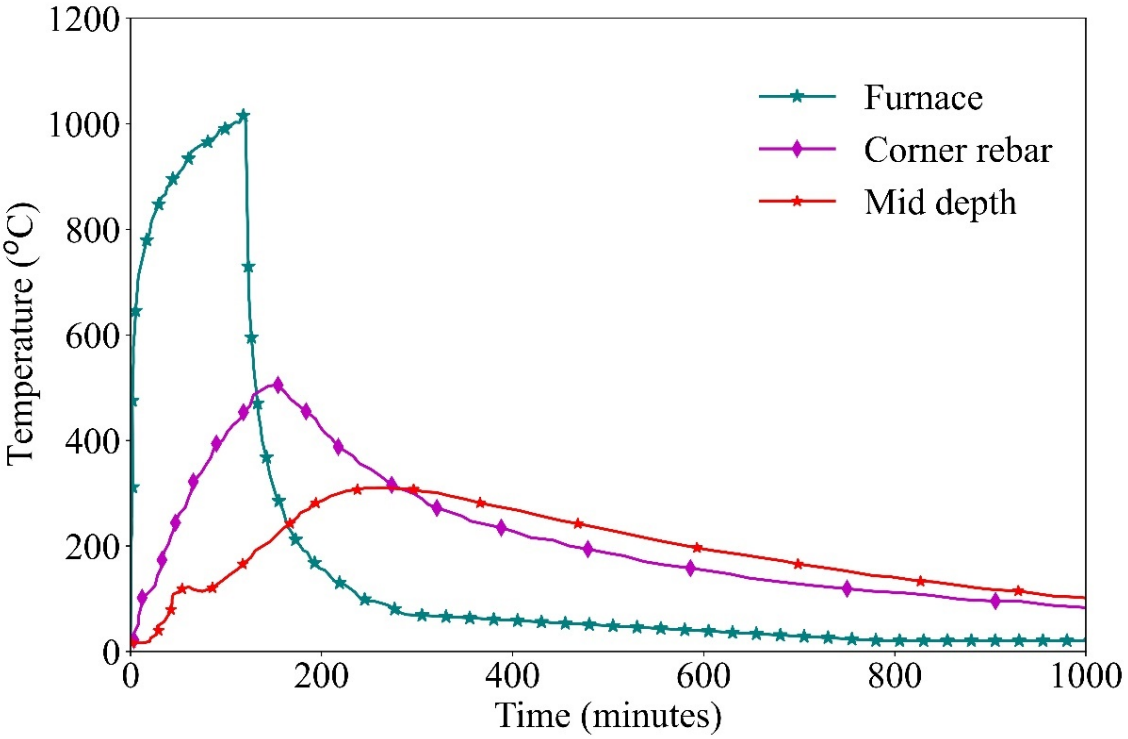
SS: simply supported.

### *4.2. Response During Fire Exposure*

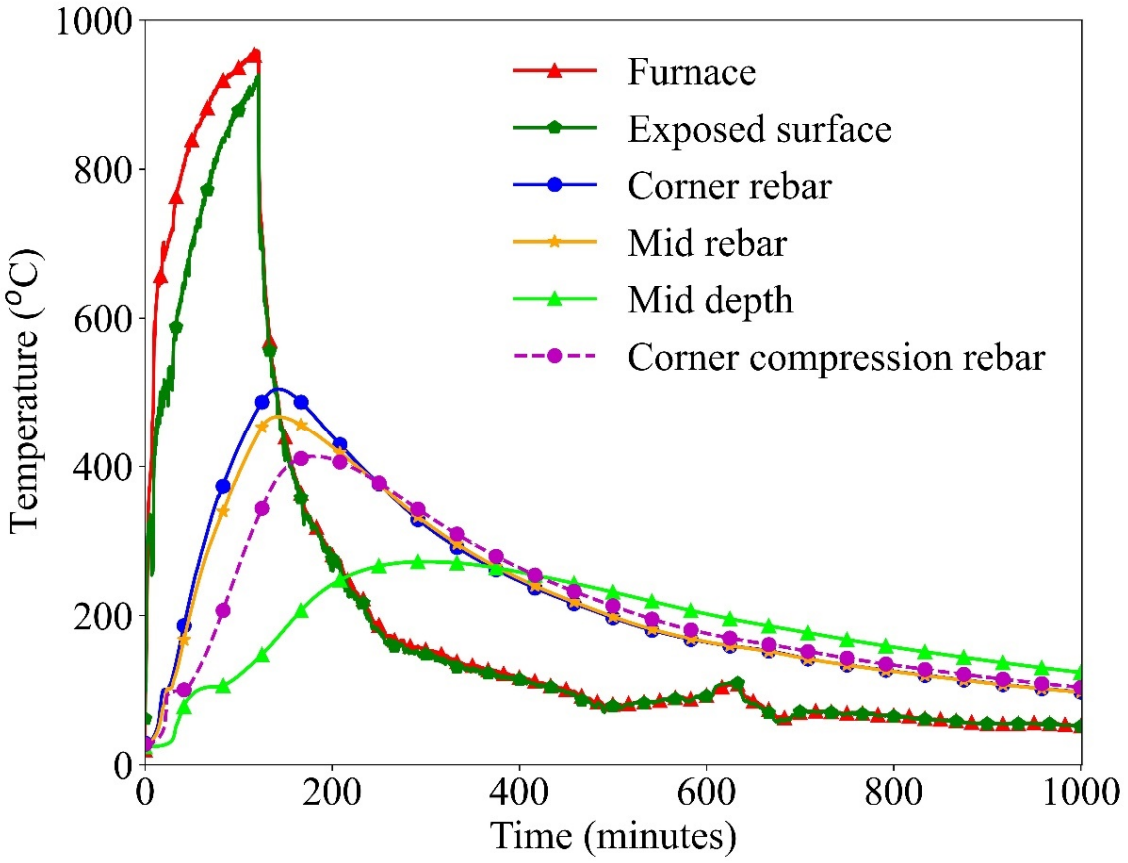
The thermal and structural responses of the tested beams were evaluated throughout the duration of fire exposure, as well as during the subsequent extended cooling phase, defined as the period between fire extinction and the return of the entire cross-section to ambient temperature. During this stage, key response parameters such as cross-sectional temperatures, mid-span deflections, spalling, and post-fire residual deformations were systematically monitored.

#### 4.2.1. Thermal Response

The thermal response of the tested B1 and TB1 beams during fire exposure is illustrated in Figure 7a,b, which shows the variation in rebar and concrete temperatures at section BB across the cross-section over time. Unlike the rapid rise in furnace (fire) temperature during the initial fire exposure duration, the temperatures within the beam cross-section remained relatively low in the early stages. A significant increase in internal temperatures was observed approximately 10 to 15 min after the start of fire exposure, by which point the furnace temperature had already exceeded 700 °C. Figure 7a shows the furnace, corner rebar, and mid-depth temperature for the B1 beam. Figure 7b shows the furnace, exposed, corner rebar, mid-rebar, mid-depth, and corner compression rebar temperatures. The slightly lower temperatures at the exposed surface (TC6) for the TB1 beam compared to the furnace are due to heat loss through radiation and convection. The temperature rise in the corner rebar (TC8) of both beams was faster than that in the mid-rebar (TC7). This is because the corner rebars experienced heat spread from the bottom and side surfaces. It was also observed that the temperature rise in the inner concrete core (TC9) was significantly slower due to the low thermal conductivity and high specific heat capacity of concrete, which reduced heat transfer to the interior core. Cross-sectional temperatures were monitored until the beam cooled back to room temperature. Notably, the temperature within the beam continued to increase even after the furnace started cooling, which can be attributed to the high thermal inertia of concrete that causes heat to redistribute and retain within the section for a longer duration. Figure 7b also shows the peak temperatures reached during the cooling phase. The mid-depth (TC9) of the beam showed a stronger influence of thermal inertia than the outer layers. As a result, the time required for the beam to cool back to ambient temperature was considerably longer than the heating duration, since the increased porosity of fire-exposed concrete reduces thermal conductivity and leads to greater heat retention. In the TB1 beam, thermocouples were also placed on the compression rebars located within the flange, and these recorded lower peak temperatures compared to the tension rebars. This behavior highlights the heat shielding effect provided by the flange, and this helps in the greater stiffness retention observed in the T-shaped beam.




(**a**)




(**b**)

**Figure 7.** (**a**) Measured cross-sectional temperatures in the B1 beam, (**b**) measured cross-sectional temperatures in the TB1 beam.

Figure 8 shows a comparison between the corner rebar (TC8) and mid-depth (TC9) temperatures of the TB1 and B1 beams. The corner rebar temperatures show similar trends in both beams, reaching a peak of 500 °C at about 150 min. However, beam B1 exhibits a mid-depth temperature nearly 15% higher than that of beam TB1. This difference is due to the presence of a flange in the TB1 beam, which serves as a heat shield, whereas the B1 beam is more uniformly exposed to heat from all sides [18]. During the cooling phase, the T-shaped (TB1) beam shows a slower decrease in cross-sectional temperature compared to the rectangular (B1) beam. This slower cooling rate represents a scenario in which the fire is allowed to decay naturally.

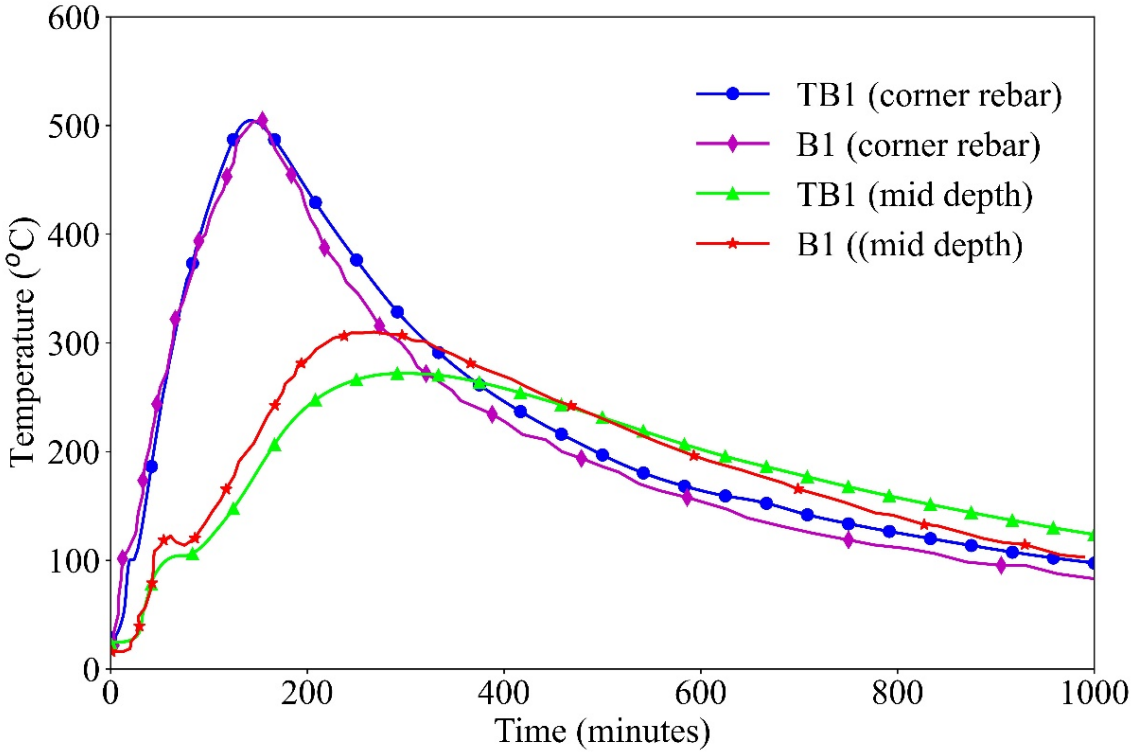



**Figure 8.** Measured corner rebar (TC8) and concrete mid-depth (TC9) temperatures as a function of fire exposure time in the tested B1 and TB1 beams (heating and cooling phases), as well as extended cool down.

Overall, the T-beam experienced marginally lower temperatures at mid-depth compared to the rectangular beam due to the presence of the flange, which acted as a heat shield. It also cooled more slowly, reflecting the combined effect of thermal inertia and the natural decay of the fire. In addition, the slower cooling in the T-beam can be partly attributed to the use of natural cooling, whereas the rectangular beam was subjected to fan-assisted cooling.

#### 4.2.2. Structural Response

Figure 9 shows a comparison between the structural response of the TB1 and B1 beams during the heating phase, cooling phase, and extended cooldown phase based on mid-span deflection measurements. Beam B1 with a rectangular section undergoes slightly higher deflection during the first 20 min of fire exposure. This is due to the applied loads having a dominant influence on deflection during the early stages of heating.

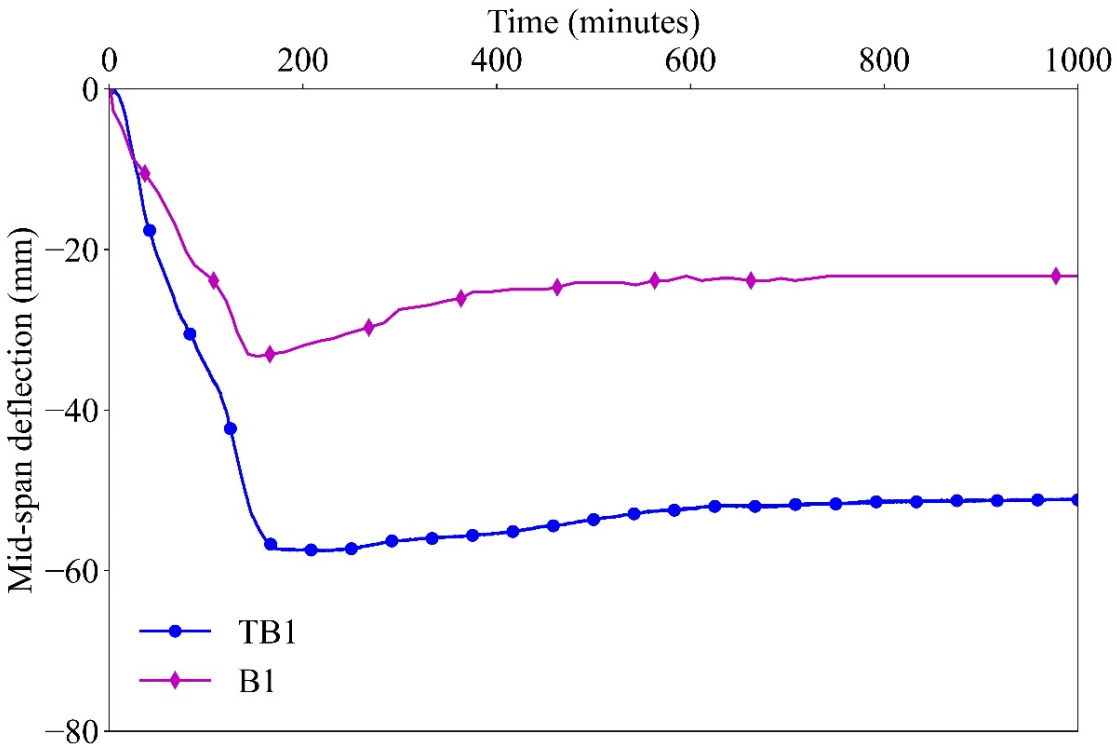



**Figure 9.** Measured deflection response at mid-span of tested RC beams during fire exposure (heating and cooling phases) and extended cooldown.

As fire exposure continues, cross-sectional temperatures rise, and the thermal gradient across the beam depth decreases because the heat gradually penetrates from the surface to the core. As a result, the temperature difference between the outer and inner regions reduces, leading to a more uniform temperature distribution within the section. Mid-span deflection increases gradually, mainly due to the degradation of mechanical properties, particularly the elastic modulus of the reinforcing steel.

Both beams were exposed to 120 min of heating following the ASTM E119 standard fire curve [19]. After 20 min, the mid-span deflection of the TB1 beam exceeds that of the B1 beam. This behavior is attributed to the reduced effective stiffness of the flange, which is directly exposed to heat on its bottom surface, resulting from rapid temperature rise and early material degradation. Additionally, the non-uniform temperature distribution between the flange and web further contributes to the loss of stiffness. The larger heat-exposed surface area of the TB1 beam, combined with its lower elastic modulus compared to the B1 beam, is also likely to have contributed to the greater deflection response. The peak mid-span deflections of the B1 and TB1 beams are 33 mm and 57 mm, respectively, occurring around 160 min. After this period, the beam deflections recover slightly, with the rectangular cross-section beam recovering faster.

The deflection trends, shown in Figure 9, indicate that mid-span deflection is strongly influenced by the peak temperature attained in the tensile reinforcement. After 120 min of heating, the deflection continues to increase as the rebar temperature remains above 400 °C. The residual deflection in both beams begins to stabilize at around 700 min, corresponding to a rebar temperature of approximately 150 °C. Therefore, the cooling-phase data from 700 to 1000 min were retained to allow the beams to further cool down and to monitor whether any additional deflection recovery or delayed deformation occurred during the stabilization stage. The final stabilized cooldown deflections for the TB1 and B1 beams are 51 mm and 23 mm, respectively.

To provide a more quantitative interpretation of stiffness degradation during heating, an effective flexural stiffness trend can be inferred from the load–deflection response. Although both beams were subjected to comparable load ratios (55% for B1 and 50% for TB1), the peak mid-span deflection of TB1 (57 mm) was approximately 73% higher than that of B1 (33 mm). At the end of the 120 min heating phase, TB1 exhibited significantly greater deflection despite similar peak rebar temperatures (~500 °C), indicating a more pronounced reduction in effective stiffness. This accelerated stiffness degradation in the T-beam can be attributed to its larger exposed surface area (approximately 17% higher) and the direct exposure of the flange soffit, which led to earlier thermal softening in the compression zone.

Furthermore, the difference in residual deformation (51 mm for TB1 versus 23 mm for B1) suggests differences in curvature distribution and compression block behavior. In the T-beam, the upward shift of the neutral axis into the flange region during heating reduced the effective compression block depth and increased tensile strain demand in the reinforcement. This resulted in larger curvature development at mid-span and greater unrecoverable deformation. In contrast, the rectangular beam maintained a more uniform compression zone, contributing to improved stiffness retention and lower residual curvature. These geometric effects, combined with thermal gradients across the flange and web, provide a mechanistic explanation for the higher deflection and residual deformation observed in the T-beam.

Table 5 presents a comparison of the key structural and thermal response parameters of the B1 and TB1 beams subjected to fire exposure. Both beams experienced similar peak rebar temperatures of 500 °C, suggesting equivalent thermal exposure. However, the TB1 beam showed a significantly higher peak mid-span displacement (57 mm) and residual deformation (47 mm) than the B1 beam (33 mm and 16 mm, respectively), indicating greater structural damage and reduced stiffness retention. The cracking moments during the pre-fire stage were comparable for both beams, with the B1 beam having a slightly higher value (38.5 kNm) than the TB1 beam (37.6 kNm). Overall, the B1 beam demonstrated better fire performance in terms of deformation control, which can be attributed to the larger exposed surface area of the TB1 beam.

**Table 5.** Summary of measured response for tested beams.

| Parameters | Beam | |
|---|---|---|
| | **B1** | **TB1** |
| Peak rebar temperature (°C) | 500 | 500 |
| Peak mid-span displacement (mm) | 33 | 57 |
| Residual deformation (mm) | 16 | 47 |
| Residual capacity (kN) | 93 | 82 |
| Cracking moment, $M_{cr}$ (kNm) | 38.5 | 37.6 |

### *4.3. Residual Response of Fire-Damaged Beams*

Both beams, B1 and TB1, did not attain failure during the entire fire exposure and extended cooling phase period. Following the cooldown, the residual capacity of the TB1 beam was evaluated by incrementally loading it to failure. The load–deflection response and failure mode were monitored during this test. Mid-span deflection for each beam was measured using LVDTs installed at the mid-span. The measured load–deflection responses for the B1 and TB1 beams are shown in Figure 10. The fire-damaged beams exhibit three distinct phases in the deflection response: an initial linear phase (A–B), the onset of yielding in the steel reinforcement (point B), and a plastic deformation phase with strain softening until failure (B–C).

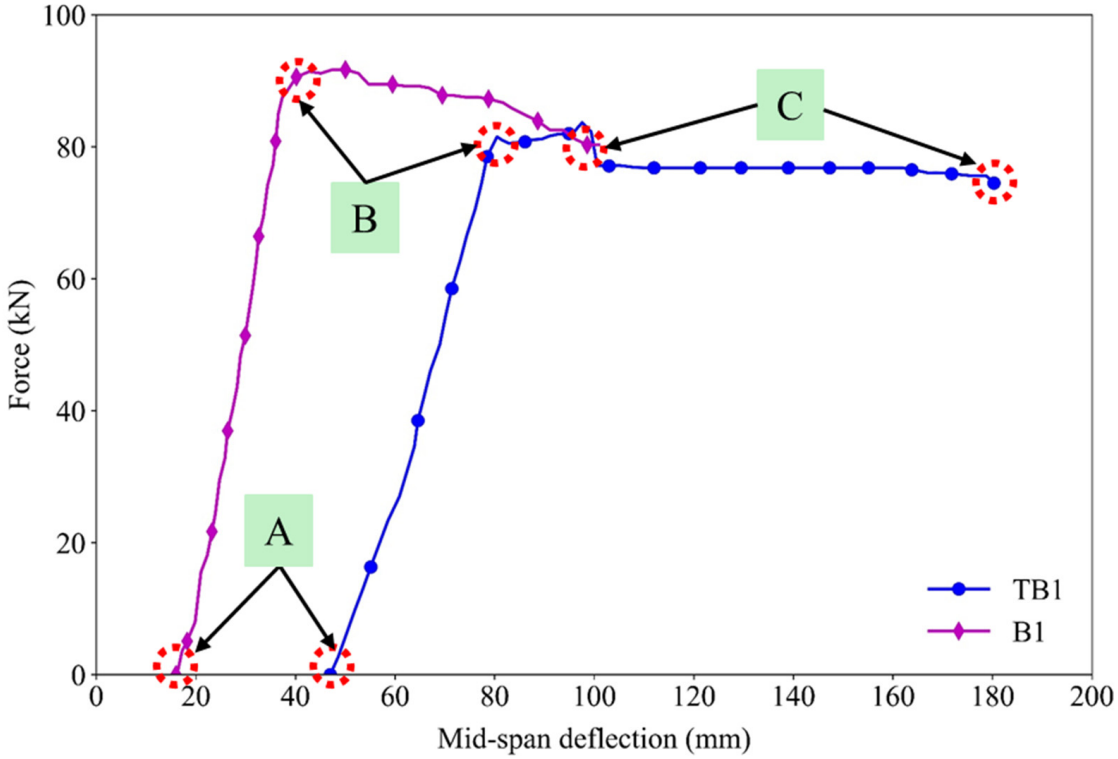



**Figure 10.** Load versus deflection response of fire-damaged reinforced concrete beams during residual capacity tests.

In the first phase (A–B in Figure 10), the load–deflection response of the fire-damaged beams follows a linear trend, consistent with the behavior of a cracked section, until the onset of yielding in the steel reinforcement. This response is attributed to extensive tensile cracking and temperature-induced material degradation in concrete and rebars during fire exposure.

The stiffness of fire-exposed RC beams is influenced by several factors, including the peak temperatures attained within the cross-section, the level of loading during fire exposure, material degradation of concrete and steel reinforcement, the area exposed to fire, and the ambient capacity of the beam. These factors collectively affect the post-fire stiffness of RC beams.

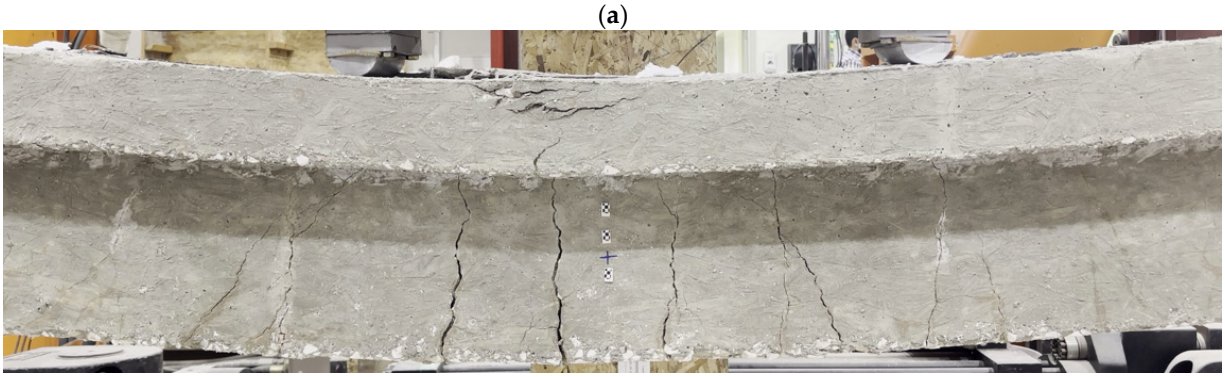
The second phase of the load–deflection response is marked by the onset of yielding in the tensile steel reinforcement. Beams B1 and TB1 both experienced similar peak rebar temperatures of 500 °C, and yielding of steel occurred at loads of 93 kN and 82 kN, respectively. The B1 beam yielded at a load approximately 13.4% higher than the TB1 beam, despite being exposed to fire for the same duration. This difference can be partly attributed to the higher room temperature capacity of the B1 beam and its smaller exposed surface area during fire exposure due to the absence of a flange.

At room temperature, the nominal moment capacities of the B1 and TB1 beams were estimated as approximately 127 kNm and 90 kNm, respectively, indicating that the B1 beam possessed about 41% higher load-carrying capacity prior to fire exposure. When compared on a normalized basis, the smaller difference in residual strength after fire (13.4%) suggests that the TB1 beam experienced a relatively lower reduction in load-bearing capacity than the B1 beam. This observation highlights the importance of considering residual performance normalized by ambient capacity when comparing fire-damaged beams with different cross-sectional configurations.

Figure 10 (B–C) shows that the delayed strain-softening in the T-beam compared to the rectangular beam is mainly due to the flange, which provides a wider compression zone and reduces stress concentration in concrete. The flange delays crushing and stabilizes post-yield behavior, allowing the beam to sustain nearly constant load over a larger deformation range [20]. Figure 11a,b show the crack patterns and failure modes of both beams after the residual capacity test. The T-beam exhibited a greater number of flexural cracks than the rectangular beam due to the presence of the flange, which shifted the neutral axis upward and caused the compression zone to lie within the flange. This shift led to higher strain in the steel reinforcement, resulting in increased flexural ductility. Consequently, more cracks developed, and several of them extended through the flange region [20]. The orientation and extent of cracking around the mid-span clearly indicate flexural failure. Since the beam ends (support zones) were not exposed to fire, the shear capacity at the supports did not reduce significantly, unlike the flexural capacity at the mid-span. The large mid-span deflection relative to the beam span further confirms a flexural (ductile) failure mode.



(**a**)



(**b**)

**Figure 11.** Crack pattern and failure mode after residual capacity test for beams: (**a**) B1, (**b**) TB1.

The experimental program included only two specimens, and the measured compressive strengths differed by approximately 23%. In addition, the rectangular beam incorporated a water-reducing agent, which may have influenced its initial stiffness and cracking behavior. Although the residual capacity calculations were based on the measured material properties of each beam to account for these differences, some inherent material variability remains. These variations may have a minor influence on both during the fire response and the post-fire residual capacity assessment; however, their effect is expected to be small relative to the dominant influence of section geometry under identical fire exposure and loading conditions. Accordingly, while geometry-driven trends are evident, the potential contribution of material variability is acknowledged as a limitation of the study.

## 5. Simplified Approach for Post-Fire Assessment

In order to further highlight the difference in residual capacity of T and rectangular beams, a simplified approach is applied to analyze the effect of cross-section on the residual response of beams. This simplified approach is based on the following assumptions:

The plane section of the beam remains unchanged before and after bending. There is no relative bond slip between the rebar and concrete during or after fire exposure. The tensile contribution of concrete in the tension zone is neglected. The residual strength using a simplified approach for RC beams after fire exposure is determined using the following procedures and is discussed in the following subsections.

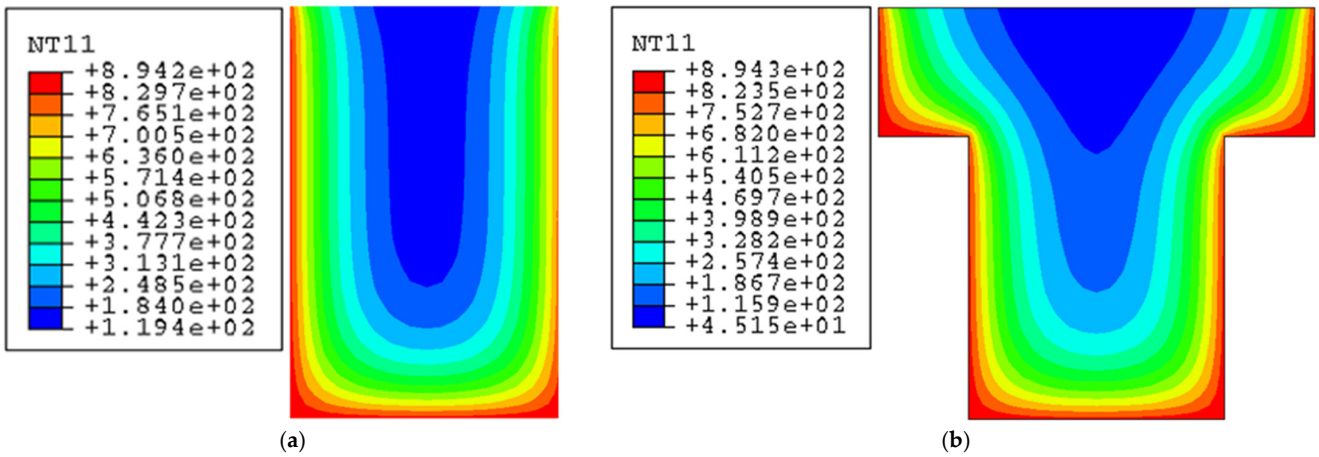
### *5.1. Concrete Cross-Section Temperature and Maximum Rebar Temperature*

The maximum temperature in the rebar and concrete cross-section can be estimated using empirical methods or heat transfer models developed utilizing finite element-based software. In this study, a heat transfer model developed in ABAQUS (2023) was used to determine the cross-sectional temperatures of the beam. The element types used to model the concrete and steel reinforcement were C3D8T and T3D2T, respectively. A mesh size of 15 mm × 15 mm was used for the concrete. These elements are capable of conducting heat through the beam model under applied transient temperatures, which were initiated at the fire-exposed surfaces.

The C3D8T element is an eight-node, thermally coupled brick element with three translational degrees of freedom in the x, y, and z directions [21]. The T3D2T element is a two-node, thermally coupled truss element used to model one-dimensional reinforcing bars or rods [21]. The interaction between concrete and reinforcement was modeled using the embedded region constraint, where the reinforcement was defined as embedded in the concrete. This constraint allows for the effective transfer of temperature from the concrete to the steel reinforcement at corresponding locations.

The fire-exposed surfaces of the C3D8T elements were used to simulate heat transfer due to convection and radiation. According to Eurocode 2 (2004) [22], a convective heat transfer coefficient of 25 W/m$^2$·°C was applied to the fire-exposed surfaces. For the unexposed surfaces, a lower coefficient of 5 W/m$^2$·°C was used to represent radiative heat exchange with the surroundings. An emissivity value of 0.5 was adopted for the fire-exposed concrete surfaces. The material properties used for the concrete and steel rebars were taken from Eurocode 2 (2004) [22].

The isotherms obtained from the heat transfer model at 120 min for the B1 and TB1 beams are shown in Figures 12a and 12b, respectively. The peak rebar temperatures predicted by the model were consistent with the temperatures measured during the fire tests.




(**a**) (**b**)

**Figure 12.** Isothermal distribution in the RC beam at 120 min: (**a**) rectangular (B1), (**b**) T-shape (TB1).

### 5.2. Residual Strength in Rebar and Concrete

An increase in cross-sectional temperature leads to a reduction in the strength of both rebar and concrete. While rebar recovers most of its strength and stiffness upon cooling, it does not regain its full strength if the peak temperature exceeds 500 °C [2,23,24]. According to Neves et al. (1996) [24] and Kodur et al. (2013) [2], the temperature-dependent residual strength of rebar can be estimated using the equation proposed in their study, as shown in Equation (1).

$$\frac{f_{yT}}{f_y} = 1 - 0.28 \times \left(\frac{T - 500}{300}\right) \leq 1 \tag{1}$$

where $f_y$, $f_{yT}$, and $T$ represent the yield strength at room temperature, yield strength at elevated temperature, and temperature of rebar, respectively. In the case of concrete, it experiences severe degradation beyond approximately 600 °C due to decomposition of hydration products and extensive microcracking. Therefore, its compressive strength is assumed to be zero when the temperature exceeds 600 °C. For temperatures less than or equal to 300 °C, the compressive strength is considered to be equal to its value at ambient conditions. The post-fire compressive strength of concrete can be estimated using a simplified representation, as proposed in analytical studies [13]. The proposed equation is a conservative but widely adopted simplification in post-fire calculation methods to avoid overestimation of compression capacity in heavily heated regions.

### 5.3. Residual Capacity Evaluation

The ACI 318 provisions are employed to determine the post-fire neutral axis depth of the beam. The moment capacity for rectangular beam B1 is calculated using Equation (2):

$$M_{nT} = f_{yT}\, A_s \left(d - \frac{\frac{f_{yT}\, A_s}{0.85\, f_c\, b_f}}{2}\right), \tag{2}$$

where $M_{nT}$, $A_s$, $f_c$, $b_f$, and $d$ represents residual moment capacity, area of rebar, compressive strength of concrete, width of flange, and effective depth, respectively.

For T-beams, two different cases are considered in the calculation of the moment capacity, depending on the location of the neutral axis. In Case I, the neutral axis lies within the flange, and the capacity is computed using Equation (2). In Case II, the neutral axis lies within the web region, and the capacity is computed using Equation (3).

Case II, when a neutral axis lies in the web, is shown as follows:

$$M_{nT} = 0.85\, K_{cF}\, f_c\, b_f\, t_f \left(\widetilde{V} + \frac{t_f}{2}\right) + 0.85\, K_{cW}\, f_c\, b_w \left(\widetilde{V}\right) \left(d - \left(\frac{\widetilde{V}}{2}\right)\right) \tag{3}$$

where $t_f$ and $b_w$ represent the thickness of the flange and the width of the web. In Equation (3), $\widetilde{V}$ is expressed as $\widetilde{V} = \frac{f_{yT}\, A_s - 0.85\, K_{cF}\, f_c\, b_f\, t_f}{0.85\, K_{cW}\, f_c\, b_w}$

$$K_{cF} = \frac{\sum_{i=1}^{r} f_{cTi} A_i}{f_c A_F}, \tag{4}$$

$$K_{cW} = \frac{\sum_{i=1}^{g} f_{cTi} A_i}{f_c A_W}, \tag{5}$$

where $K_{cF}$ and $K_{cW}$ represent the equivalent strength reduction factors for the flange and web, respectively. $r$ and $g$ are the total number of elements for the flange and web, respectively. $f_{cTi}$ represent the residual compressive strength of concrete at the $i$th element after fire exposure. $A_i$ denotes the area of the $i$th element. $A_F$ and $A_W$ represent the area

of the flange and the area of the web, respectively. Thus, the summations $\sum_{i=1}^{r} f_{cTi} A_i$ and $\sum_{i=1}^{g} f_{cTi} A_i$ represent the post-fire effective compressive capacity of that region. The denominators $f_c A_F$ and $f_c A_w$ correspond to the ambient capacity of the flange and web, respectively. Using these parameters, the depth of neutral axis ($\gamma$) can be determined by dividing the height of the stress block ($\alpha$) by the block parameter ($\beta$), where $\beta$ is obtained from ACI 318 and $\alpha$ is calculated as $(\frac{f_{yT}\ A_s}{0.85\ K_{cF}\ f_c\ b_f})$.

Table 6 presents a comparison of the predicted and measured residual strengths of the rectangular (B1) and T-shaped (TB1) beams. Both beams were exposed to fire following the ASTM E119 standard for 120 min. The peak rebar temperatures from both the measured and predicted values are in close agreement, indicating good accuracy of the heat transfer model.

**Table 6.** Comparison of predicted and measured residual strength in fire-exposed RC beams.

| Beam | Fire Exposure Time (min) | Measured Residual Value | | | Predicted Residual Value | | |
|---|---|---|---|---|---|---|---|
| | | Maximum Rebar Temperature (°C) | Moment Capacity (kNm) | Load (kN) | Maximum Rebar Temperature (°C) | Moment Capacity (kNm) | Load (kN) |
| B1 | 120 | 500 | 130.2 | 93 | 500 | 119.8 | 85.6 |
| TB1 | 120 | 500 | 114.8 | 82 | 500 | 88.2 | 63 |

The validity of the proposed approach was evaluated by comparing the predicted moment capacities with the values obtained from the residual strength tests. The predicted residual flexural capacities for both beams are conservative, ranging from approximately 10% to 20% lower than the measured values. This difference is mainly due to the fact that the proposed approach does not account for strain hardening, similar to the approach adapted in room temperature design, as specified in ACI 318 (ACI, 2008) [17]. Strain hardening in rebars can enhance the flexural capacity of reinforced concrete beams at ambient conditions [2].

As shown in Table 6, the predicted residual capacity of the TB1 beam is approximately 20% lower than the predicted value, while for the B1 beam, the predicted value is about 8% lower. The larger difference in the TB1 beam can be attributed to a greater contribution from strain hardening in its reinforcement. The difference between the predicted and measured flexural capacities generally decreases with increasing rebar temperature [2]. This is because at higher temperatures, as steel softens, the effect of strain hardening reduces, making the predicted capacity closer to the measured value. Overall, the proposed method can estimate the residual load-carrying capacity of fire-exposed RC beams.

The simplified model does not explicitly incorporate post-fire strain hardening of reinforcement. Inclusion of even modest post-yield strength enhancement could increase the predicted moment capacity by a few percent, thereby contributing to the conservative underprediction observed in the analytical results. For the T-beam, the larger discrepancy is further associated with flange compression block behavior. During heating, the upward shift of the neutral axis into the flange reduces the effective compression block depth and increases curvature demand. These geometric and thermal interaction effects are not fully captured by the simplified rectangular compression block idealization, which may underestimate the residual compression contribution of the flange.

## 6. Application of the Simplified Approach in a Parametric Study

The simplified approach is further applied to carry out a parametric study on rectangular and T-shaped reinforced concrete (RC) beams with varying cross-sectional dimensions. The geometric and material properties of the beams are presented in Table 7. In Table 7,

beams BI and BII represent rectangular beams, while beams BIII, BIV, BV, BVI, and BVII represent T-shaped beams.

**Table 7.** Properties for RC beams used in the parametric study.

| Property | Beam | | | | | | |
|---|---|---|---|---|---|---|---|
| | Rectangular | | T-Shape | | | | |
| | BI | BII | BIII | BIV | BV | BVI | BVII |
| Length (m) | 3.96 | | 3.96 | | | | |
| Cross-sectional (mm) | 210 × 350 | 300 × 500 | Flange: 372 × 127 Web: 210 × 223 | Flange: 532 × 127 Web: 300 × 373 | Flange: 532 × 127 Web: 240 × 373 | Flange: 532 × 80 Web: 300 × 420 | Flange: 532 × 80 Web: 240 × 420 |
| Longitudinal rebar diameter | Top: 2–14 mm ϕ Bottom: 3–20 mm ϕ | | Top: 4–14 mm ϕ Bottom: 3–20 mm ϕ | | | | |
| Transverse rebar diameter | - | - | 10 mm ϕ @ 305 mm c/c | | | | |
| Stirrup rebar diameter | 10 mm ϕ @ 150 mm c/c | | 10 mm ϕ @ 150 mm c/c | | | | |
| Concrete cover (mm) | 40 | | 40 | | | | |
| $f'_c$ (MPa) | 30 | | 30 | | | | |
| $f'_y$ (MPa) | 400 | | 400 | | | | |

Beams BII, BIV, and BV also share the same overall depth. Beam BIV has the same web width as beam BII, whereas beam BV has a 20% reduction in web width to evaluate the effect of reduced web thickness. Beams BVI and BVII, which are similar to beams BIV and BV, respectively, have a 37% reduction in flange thickness. All beams were exposed to the three sides of the ASTM E119 standard fire curve for durations of 60, 90, and 120 min. This parametric study enables the evaluation of how variations in web thickness and flange depth influence the residual capacity of beams with the same overall depth.

Table 8 presents the results of the parametric study for rectangular and T-shaped beams with varying cross-sectional properties under different fire exposure durations. For beams with similar depth but different cross-sections, the moment capacity at room temperature ranges from 96.05 kNm (beam BI) to 160.64 kNm (beams BIV to BVII).

After 60 min of ASTM E119 fire exposure, the peak reinforcement temperature in all beams reached approximately 298 °C. At this temperature, the reductions in residual flexural capacity were 2% and 0.5% for beams BI and BIII, 1%, 0.2%, and 0.2% for beams BII, BIV, and BV, and 0.5% for beams BVI and BVII. When the exposure duration increased to 90 min, the peak rebar temperature rose to 420 °C, resulting in further capacity losses of 6% and 2% for beams BI and BIII, 2%, 0.4%, and 0.4% for beams BII, BIV, and BV, and 1% for beams BVI and BVII. After 120 min, the rebar temperature reached about 516 °C, and the combined degradation of concrete and steel led to larger capacity reductions of 8% and 3% for beams BI and BIII, 3%, 2%, and 2% for beams BII, BIV, and BV, and 3% for beams BVI and BVII. Overall, the results indicate that the reduction in residual flexural capacity remains relatively small even after 120 min of ASTM E119 fire exposure.

This modest reduction is consistent with the predicted post-fire material degradation at this exposure level. At 120 min, the peak rebar temperature of approximately 516 °C corresponds to a residual yield strength of about $0.985 f_y$ based on Equation (1), indicating only limited steel strength loss. Similarly, the post-fire concrete strength ranges from approximately $0.68 f_c$ to $0.86 f_c$, depending on the cross-section, which is determined by estimating the average temperature of the compression block above the neutral axis and applying the corresponding reduction relation. Since the governing reduction factors for both steel and concrete remain moderate at this stage, the resulting decrease in residual flexural capacity is correspondingly limited, as reflected in Table 8.

**Table 8.** Results for RC beams used in the parametric study.

| Beam Type | Moment Capacity at Room Temperature (kNm) | Time (min) | Peak Rebar Temperature (°C) | Predicted Residual Capacity (kNm) |
|---|---|---|---|---|
| Beam BI (Rectangular) | 96.05 | 60 | 298 | 94.16 |
| | | 90 | 420 | 90.70 |
| | | 120 | 516 | 88.79 |
| Beam BII (Rectangular) | 156.6 | 60 | 298 | 155.09 |
| | | 90 | 420 | 154.35 |
| | | 120 | 516 | 151.96 |
| Beam BIII (T-shape) | 101.84 | 60 | 298 | 101.3 |
| | | 90 | 420 | 100.41 |
| | | 120 | 516 | 98.75 |
| Beam BIV (T-shape) | 160.64 | 60 | 298 | 160.36 |
| | | 90 | 420 | 159.96 |
| | | 120 | 516 | 157.50 |
| Beam BV (T-shape) | 160.64 | 60 | 298 | 160.26 |
| | | 90 | 420 | 159.94 |
| | | 120 | 516 | 157.44 |
| Beam BVI (T-shape) | 160.64 | 60 | 298 | 159.77 |
| | | 90 | 420 | 159.41 |
| | | 120 | 516 | 156.4 |
| Beam BVII (T-shape) | 160.64 | 60 | 298 | 159.85 |
| | | 90 | 420 | 159.3 |
| | | 120 | 516 | 156.2 |

The predicted responses consistently show lower capacity degradation in T-shaped beams compared to rectangular beams, in agreement with the experimental observations. Because all beams were modeled with a constant 40 mm concrete cover, the peak reinforcement temperatures remained nearly identical across different cross-sections, confirming that reinforcement heating is governed primarily by cover thickness rather than section geometry. This observation aligns with the findings of Vishal and Satyanarayanan (2022) [25], who also reported that cover thickness plays a dominant role in controlling reinforcement temperature under fire exposure. Therefore, differences in residual capacity arise mainly from variations in compression block geometry and stiffness distribution. These results indicate that appropriate proportioning of flange and web dimensions in T-beams can enhance post-fire residual strength without altering cover depth, providing practical guidance for structural fire design and assessment.

## 7. Conclusions

The experimental investigation provides valuable insights into the fire behavior and post-fire performance of rectangular and T-shaped reinforced concrete beams. Based on the measured thermal and structural responses, the following conclusions are drawn:

1. Both rectangular and T-shaped beams experience similar peak rebar temperature because reinforcement heating is governed by concrete cover, and not by the cross-sectional geometry.
2. The T-shaped beam exhibited significantly higher mid-span deflection during fire exposure despite similar peak rebar temperatures. This is mainly due to a larger exposed surface area, which accelerates heat transfer and stiffness degradation.
3. The T-shaped beam developed more and wider flexural cracks in the post-fire residual test. This is mainly due to the upward shift of the neutral axis, which reduced the compression zone and increased tensile strain in the reinforcement, leading to greater crack formation.
4. Rebar temperature is dictated primarily by cover thickness, but relative residual capacity still differs between different cross-sections due to differences in compression block geometry and stiffness distribution. Proper proportioning of flange and web geometry (thicker flange and thinner web) of T-beams can offset geometric vulnerabilities to fire-induced stiffness degradation, and this can achieve higher post-fire residual capacity.
5. The simplified method proposed here provides conservative estimates of post-fire residual capacity, typically within 10–20% of detailed numerical predictions, making it suitable for rapid post-fire evaluations where detailed analysis is impractical.
6. Fire damage evaluation solely based on peak rebar temperatures is inadequate. A comprehensive assessment incorporating residual deflection, stiffness degradation, and crack mapping, with due consideration to sectional geometry (rectangular or T), is essential for developing effective post-fire residual capacity assessment and rehabilitation strategies.

**Author Contributions:** M.K.S.: writing—review and editing, writing—original draft, validation, software, methodology, investigation, formal analysis, and data curation. P.B.: writing—review and editing, validation, methodology, and investigation. V.A.M.: writing—review and editing, visualization, supervision, investigation, and conceptualization. H.K.: writing—review and editing and validation. V.K.R.K.: writing—review and editing, visualization, validation, supervision, resources, project administration, methodology, investigation, funding acquisition, formal analysis, and conceptualization. All authors have read and agreed to the published version of the manuscript.

**Funding:** This research received no external funding.

**Data Availability Statement:** The data supporting the findings of this study are available from the corresponding author upon reasonable request.

**Acknowledgments:** Funding received from the United States-India Educational Foundation (USIEF) to Vasant Matsagar under the Fulbright-Kalam Climate Fellowship for Academic and Professional Excellence is gratefully acknowledged. The opinions expressed in this manuscript are those of the authors and not those of the funding agency.

**Conflicts of Interest:** Author Pratik Bhatt was employed by the company Engineering Systems Inc. (ESi). The remaining authors declare that the research was conducted in the absence of any commercial or financial relationships that could be construed as a potential conflict of interest.

## References

1. International Code Council, Inc. (ICC). *International Building Code*; International Code Council, Inc. (Formerly BOCA, ICBO and SBCCI): Washington, DC, USA, 2006.
2. Kodur, V.K.R.; Raut, N.K.; Mao, X.Y.; Khaliq, W. Simplified approach for evaluating residual strength of fire-exposed reinforced concrete columns. *Mater. Struct.* **2013**, *46*, 2059–2075. [CrossRef]
3. Alonso, C. Assessment of post-fire reinforced concrete structures. Determination of depth of temperature penetration and associated damage. In *Concrete Repair, Rehabilitation and Retrofitting II*; CRC Press: Cape Town, South Africa, 2008; pp. 217–218.

4. Gil, A.; Kodur, V.; Pacheco, F.; Schneider, D.; Christ, R.; Tutikian, B. Post-fire assessment and retrofitting of concrete buildings: Case study. *ACI Struct. J.* **2022**, *119*, 57–67. [CrossRef]
5. Kodur, V.K.; Agrawal, A. Critical factors governing the residual response of reinforced concrete beams exposed to fire. *Fire Technol.* **2016**, *52*, 967–993. [CrossRef]
6. Zheng, W.Z.; Hou, X.M.; Wang, Y. Progress and prospect of fire resistance of reinforced concrete and prestressed concrete structures. *J. Harbin Inst. Technol.* **2016**, *48*, 1–18.
7. Bai, L.L.; Wang, Z.Q. Residual bearing capacity of reinforced concrete member after exposure to high temperature. *Adv. Mater. Res.* **2012**, *368*, 577–581. [CrossRef]
8. Choi, E.G.; Shin, Y.S.; Kim, H.S. Structural damage evaluation of reinforced concrete beams exposed to high temperatures. *J. Fire Prot. Eng.* **2013**, *23*, 135–151. [CrossRef]
9. Agrawal, A.; Kodur, V.K.R. A novel experimental approach for evaluating residual capacity of fire damaged concrete members. *Fire Technol.* **2020**, *56*, 715–735. [CrossRef]
10. Liu, C.; Lu, X.; Ba, G.; Liu, H.; Miao, J. Influence of loading conditions on the residual flexural capacity of reinforced concrete T-beams after fire exposure. *KSCE J. Civ. Eng.* **2021**, *25*, 4710–4723. [CrossRef]
11. Liu, C.W.; Mao, J.Y.; Dong, K.; Miao, J.J.; Gu, Z.J.; Li, L.H. Calculation Method of the Residual Bearing Capacities of Concrete T-Shaped Beams Considering the Effect of Fire Cracks. *Fire Technol.* **2023**, *59*, 305–329. [CrossRef]
12. Awad, Y.; Kohail, M.; Khalaf, M.A.; Ali, Y.A. Effect of fire extinguishing techniques on the strength of RC columns. *Asian J. Civ. Eng.* **2022**, *23*, 113–123. [CrossRef]
13. Wang, Z.; Xu, C.; Chen, M.; Sun, J.; Zhou, H.; Zhou, Y. Experimental Test and Analytical Calculation on Residual Strength of Prestressed Concrete T-Beams After Fire. *Buildings* **2024**, *14*, 3579. [CrossRef]
14. Kodur, V.K.R.; Agrawal, A. An approach for evaluating residual capacity of reinforced concrete beams exposed to fire. *Eng. Struct.* **2016**, *110*, 293–306. [CrossRef]
15. Nassif, A. Postfire full stress-strain response of fire-damaged concrete. *Fire Mater. Int. J.* **2006**, *30*, 323–332. [CrossRef]
16. *ACI 318-19/318R-19*; Building Code Requirements for Structural Concrete and Commentary. American Concrete Institute: Farmington Hills, MI, USA, 2019.
17. *ACI 318-08*; Building Code Requirements for Structural Concrete (ACI 318-08) and Commentary. American Concrete Institute: Farmington Hills, MI, USA, 2008.
18. Xu, Y.Y.; Wu, B.; Jiang, M.; Huang, X. Experimental study on residual flexural behavior of reinforced concrete beams after exposure to fire. *Adv. Mater. Res.* **2012**, *457*, 183–187. [CrossRef]
19. *ASTM E119*; Standard Test Methods for Determining Effects of Large Hydrocarbon Pool Fires on Structural Members and Assemblies. American Society for Testing and Materials: West Conshohocken, PA, USA, 2008.
20. Kamonna, H.H.; Shakir, Q.M.; Al-Tameemi, H.A. Behavior of high-strength self-consolidated reinforced concrete t-deep beams. *Open Constr. Build. Technol. J.* **2020**, *14*, 51–69. [CrossRef]
21. Dassault Systèmes. *Abaqus/CAE User's Guide, Version 2016*; Dassault Systèmes Simulia Corp.: Providence, RI, USA, 2016.
22. *EN 1992-1-1:2004*; Eurocode 2: Design of Concrete Structures—Part 1-1: General Rules and Rules for Buildings. British Standards Institution: London, UK, 2004.
23. Edwards, W.T.; Gamble, W.L. Strength of grade 60 reinforcing bars after exposure to fire temperatures. *Concr. Int.* **1986**, *8*, 17–19.
24. Neves, I.C.; Rodrigues, J.P.C.; Loureiro, A.D.P. Mechanical properties of reinforcing and prestressing steels after heating. *J. Mater. Civ. Eng.* **1996**, *8*, 189–194. [CrossRef]
25. Vishal, M.; Satyanarayanan, K.S. Study on optimum concrete cover thickness in RC beam and columns under high temperature. *J. Struct. Fire Eng.* **2023**, *14*, 461–480. [CrossRef]


**Disclaimer/Publisher's Note:** The statements, opinions and data contained in all publications are solely those of the individual author(s) and contributor(s) and not of MDPI and/or the editor(s). MDPI and/or the editor(s) disclaim responsibility for any injury to people or property resulting from any ideas, methods, instructions or products referred to in the content.